NANO · MICRO
small

Supporting Information

for *Small*, DOI 10.1002/smll.202302274

Vapor-Phase Synthesis of Molecularly Imprinted Polymers on Nanostructured Materials at Room-Temperature

Elisabetta Mazzotta, Tiziano Di Giulio, Stefano Mariani, Martina Corsi, Cosimino Malitesta and Giuseppe Barillaro**

Supporting Information

Synthesis of Molecularly Imprinted Polymers on Nanostructured Materials via Room-Temperature Vapor-Phase Polymerization for Protein Sensing

Elisabetta Mazzotta, Tiziano Di Giulio, Stefano Mariani, Martina Corsi, Cosimino Malitesta and Giuseppe Barillaro**

Prof. Elisabetta Mazzotta, Dr. Tiziano Di Giulio, Prof. Cosimino Malitesta
Laboratory of Analytical Chemistry, Department of Biological and Environmental Sciences and Technologies (Di.S.Te.B.A.), University of Salento, via Monteroni, 73100 Lecce (Italy)

Dr. Stefano Mariani, Martina Corsi, Prof. Giuseppe Barillaro
Information Engineering Department, University of Pisa, via G. Caruso 16, 56122 Pisa (Italy)

E-mail: elisabetta.mazzotta@unisalento.it, giuseppe.barillaro@unipi.it

Methods

Materials and chemicals

All chemicals were of analytical grade and were used as received. Ultra-pure water (conductivity <0.1μS/cm) was used.

The chemical reagents used included (3-aminopropyl)triethoxysilane (APTES), 99%, glutaraldehyde solution II grade, 25%, human hemoglobin (HHb), lysozyme from chicken egg white lyophilized powder (Lyz), human serum albumin (HSA), cytochrome C (Cyt C), obtained from Sigma-Aldrich (St. Louis, MO, USA). Iron chloride, sodium hydroxide, monosodium phosphate (MSP), NaH_2PO_4, and disodium phosphate (DSP), Na_2HPO_4, were provided from Honeywell Fluka (College Park, GA, USA).

All solutions (except APTES) were prepared in ultra-pure water. Phosphate buffer saline (PBS) solutions (50 mM, pH 7.4), were prepared by dissolution of the commercial MSP and DSP in appropriate proportions, adding NaOH 5 M to adjust the final pH.

2% APTES solutions (v/v) were prepared in toluene. Stock solution of HHb (8 mg mL^{-1}) were freshly prepared in PBS and were diluted for obtaining HHb standard solution at different concentrations (from 0.1 to 8 mg mL^{-1}) for rebinding experiments. Solutions of Lyz, HSA and CytC, were freshly prepared in PBS in the same way, before their use. The artificial serum sample used for HHb detection tests was prepared according to a protocol reported in literature[1]. It consisted of 111 mM NaCl, 29 mM $NaHCO_3$, 2.2 mM K_2HPO_4, 0.8 mM $MgCl_2 \cdot 6H_2O$, 2.5 mM urea and 4.7 mM glucose. Plasma from human was purchased from Sigma Aldrich.

Silicon boron-doped wafers (p++ type) with resistivity of 0.8 - 1.2 mΩ×cm, orientation <100>, were purchased from Siltronix Silicon Technologies (France). Aqueous hydrofluoric acid (HF, 48%), sodium hydroxide (NaOH, 98%) were purchased from Sigma Aldrich

(Germany). Absolute ethanol (EtOH, 99.9%), and diethyl ether (Et_2O, > 99%), were purchased from Carlo Erba Reagents (Italy).

Fabrication of PSi scaffolds

Porous silicon (PSi) scaffolds were prepared by anodic etching of p-type silicon square wafer samples (1.5 × 1.5 cm^2) using 2 mL of solution HF:EtOH (3:1 v/v). A custom-made Teflon cell (circular working area of 0.567 cm^2) with platinum wire cathode and aluminium flat anode was used for electrochemical anodization of the silicon substrate. A source measurement unit (SMU, Keithley 2602A) was used to set the etching current and measure the voltage between anode and cathode.

A sacrificial PSi layer was etched at 250 mA cm^{-2} current density for 15 s, rinsed with EtOH for 120 s to remove residual HF, dissolved in a solution NaOH(1M):EtOH (9:1 v/v) for 120 s to achieve the complete removal of PSi leaving an increased surface roughness able to increase the pores size[2], and finally rinsed with DIW and EtOH to remove the dissolving solution. The nPSi interferometer was then etched with a constant current density of 250 mA cm^{-2} for 40 s, to obtain a porous layer with ~4.1 μm thickness and ~75 % porosity. Eventually, the nPSi sample was rinsed with EtOH for 120 s and Et_2O for 60 s to obtain a crack-free nPSi layer. Thermal oxidation of the PSi interferometer was carried out in a muffle furnace (ZB 1, ASAL, Italy) at 750 °C for 1 h (ramp-up/ramp-down 12 °C min^{-1}) in room atmosphere.

Optical characterization of PSi scaffolds

Reflectance spectra of the PSi interferometers were acquired in air (both before and after oxidation) in the wavelength range [400−1000 nm] using an optical setup consisting of a UV−VIS spectrometer (SM242 SP) provided by Spectral products, a bifurcated fiber-optic

probe (QR200−7-VIS-BX), and a halogen lamp source (HL-2000) purchased from Ocean Optics (USA). Light exiting the halogen lamp source is fed orthogonally onto the PSi surface through one arm of the fiber-optic probe; the light reflected from the PSi layer is collected into a UV−VIS spectrometer through the other arm of the fiber-optic probe. Acquisition parameters for reflection spectra were: integration time 15 ms, average scan number 10, boxcar width 5, with the spectrometer working in photon counts mode. Porosity of as-prepared PSi interferometers was estimated by best-fitting of the reflectance spectra of PSi layers acquired before oxidation, using a home-made software (Matlab, MathWorks, USA)[3].

FFT reflectance spectroscopy

FFT of the reflectance spectra of PSi interferometers was performed to calculate the EOT values, namely, 2nL, where n = effective refractive index and L = thickness of the PSi layer, using a home-made software (Matlab, MathWorks, USA). The wavelength axis of the reflectance spectrum was first inverted (x axis changed from wavelength to 1/wavelength) to obtain a wavenumber axis. A cubic-spline interpolation of reflectance data was then carried out to obtain a dataset (reflection, wavenumber) spaced evenly (sample-to-sample distance $8.57 \times 10{-}7$ nm−1). A Hanning window was applied to the reflectance spectrum, which was zero padded to 224. Eventually, application of the FFT algorithm to the zero- padded reflectance spectrum yielded the Fourier transform amplitude and phase (y axis in the Fourier transform domain) as a function of 1/wavenumber (x axis in the Fourier transform domain), with spatial resolution of about 0.07 nm. The EOT value is obtained as the value of the 1/wavenumber axis (x axis) in the Fourier transform domain for which the main peak in the Fourier transform amplitude (y axis) occurs.

Liquid-phase deposition of PPy in $PSiO_2$ scaffolds

Liquid-phase deposition of Polypyrrole (PPy) on $PSiO_2$ substrate was carried out slightly modifying a protocol reported in literature[4,5]. $PSiO_2$ samples were immersed in 0.1 M $FeCl_3$ solution for 30 min to allow oxidizing agent permeation into the nanostructured layer of PSi. Then, the samples were immersed in a solution of Py 0.1 M, for different time intervals (1, 2, 5, 8 h).

Vapor-phase PPy deposition of PPy in $PSiO_2$ scaffolds

Vapor-phase polymerization of PPy was carried out slightly modifying a protocol reported in literature[6,7]. The $PSiO_2$ samples were immersed in a $FeCl_3$-ethanol solution (0.5% wt/v) for 20 min. After taking the samples out from the solution and gently drying them with a N_2 flow, the $PSiO_2$ samples were placed in a closed chamber saturated with pyrrole vapors for different time intervals (1, 2, 5, 8 h), at room temperature and atmospheric pressure. The samples were repeatedly rinsed with water (5 min) to remove unreacted monomer, then with ethanol, and dried under a N_2 flow.

Morphological and compositional characterization of PSi and $PSiO_2$ scaffolds before and after PPy polymerization

Morphological and compositional characterization of PSi and $PSiO_2$ scaffolds before and after PPy deposition were carried out using a scanning electron microscope (FE-SEM, FEI Quanta 450 ESEM FEG) equipped with an energy-dispersive microanalytic system (EDX, Bruker, QUANTAX XFlash Detector 6|10 for EDX analysis). SEM and EDX analysis were performed on cross-sections of samples with a 10 kV acceleration voltage at various magnifications. Distribution of the pore diameters was obtained from the analysis of top-view SEM images with Gwyddion software.

XPS characterization

XPS measurements were recorded with an AXIS ULTRA DLD (Kratos Analytical) photoelectron spectrometer using a monochromatic AlKα source (1486.6 eV) operated at 150 W (10 kV, 15 mA). Base pressure in the analysis chamber was 5.3 x 10-9 torr. Survey scan spectra were recorded using a pass energy of 160 eV and a 1 eV step. High resolution spectra were acquired using a pass energy of 20 eV and a 0.1 eV step. In each case the area of analysis was about 700 μm x 300 μm. During the data acquisition a system of neutralization of the charge has been used. Processing of the spectra was accomplished by CasaXPS Release 2.3.16 software. The binding energy (BE) scale was referenced to the Au 4f7/2 peak at 84.0 eV. For the analysis of high resolution spectra all peaks were fitted using Shirley background and GL(30) lineshape (a combination of Gaussian 70% and Lorentzian 30%). For quantitative analysis, the relative sensitivity factors present in the library of CasaXPS for the areas of the signals were used. Surface charging was corrected considering adventitious C 1s (binding energies (BE) = 285 eV).

HHb anchoring

The protein immobilization on $PSiO_2$ scaffolds was based on the covalent anchoring of HHb protein and involves a preliminary functionalization of silicon surface with a suitable linker. Specifically, $PSiO_2$ samples were immersed in a solution of APTES prepared in toluene (2%, v/v) for 30 min at 55°C [8–10], then washed with MeOH for 5 min and rinsed with water and EtOH. Next, the samples were immersed in 5% (v/v) glutaraldehyde solutions prepared in PBS, pH 7.4, for 2 h[11,12]. Protein anchoring was carried out by drop casting 100 μL of a solution of HHb (1 mg mL^{-1}) prepared in PBS, pH 7.4 onto the functionalized $PSiO_2$ scaffolds, then left incubating for 2 hours at room temperature.

MIP synthesis by PPy vapor-phase deposition

MIP films for HHb (referred to as "dry vapor-phase MIP") were prepared by PPy vapor-phase deposition for 8 hours on $PSiO_2$ scaffolds preliminarily functionalized with HHb, as detailed in section "*Vapor-phase PPy deposition of PPy in $PSiO_2$ scaffolds*", and subsequent removal of HHb molecules from the polymer matrix by washing (1 h, stirring) the PPy-coated scaffolds in 50 mM HCl solution prepared in water. The washing step was repeated, if necessary, until a stable reflectance spectrum of the MIP-coated $PSiO_2$ scaffolds was achieved.

Further MIP films for HHb (referred to as "wet vapor-phase MIP") were achieved by vapor-phase deposition (at room temperature and atmospheric pressure) of PPy on $PSiO_2$ scaffolds preliminarily functionalized with HHb in the presence of a small water volume in the evaporation chamber together with pyrrole, to ensure saturation of the evaporation chamber with water and pyrrole vapors. After polymerization, the PPy-coated scaffolds were washed as described above for HHb removal.

Not imprinted polymer (NIP) was prepared by 8 hours PPy deposition on $PSiO_2$ substrate preliminarily functionalized with APTES and glutaraldehyde only.

HHb rebinding tests

MIP-functionalized $PSiO_2$ samples were tested with increasing concentrations of HHb (0.1- 8 mg mL^{-1}). Freshly prepared HHb solutions (100 μL) prepared in PBS at pH 7.4 were drop cast on the MIP-functionalized $PSiO_2$ scaffolds and incubated for 1 h. After incubation, the samples were rinsed with water (5 min) under stirring (200 rpm), with EtOH, and dried under a N_2 flow. Then, reflectance spectra were recorded on the so-processed $PSiO_2$ scaffolds for each HHb concentration tested. All tests were performed in triplicate. MIP and NIP sensitivity values were estimated from the slope of the calibration curves.

Rebinding tests were also performed using complex real matrices, namely, plasma from human and synthetic serum, to evaluate the potential use of the MIP-$PSiO_2$ sensor for clinical purposes. HHb stock solution was spiked in plasma and serum samples for rebinding experiments, performed under the same conditions used for calibration experiments with buffer solution.

Derivation of the MIP association constant using the Langmuir-Freundlich isotherm model

The MIP association constant (K_0**)** was estimated using Langmuir-Freundlich isotherm model according to the following equations:

$$\log\frac{S}{S_{max}-S} = \log a + m \log C \qquad (1)$$

$$K_0 = a^{\frac{1}{m}} \qquad (2)$$

where *S* is the sensor output signal, S_{max} is the maximum value of the sensor output, *a* is related to the median binding affinity, *m* is the heterogeneity index, *C* is the analyte concentration [13,14]. The fitting parameters S_{max}, *a*, *m* were extracted by best-fitting the experimental calibration curve recorded on MIP sensors in the range 0.1 to 8 mg mL^{-1} of HHb using Eq. (1).

Selectivity, repeatability and stability experiments

Selectivity of the MIP was evaluated by testing the MIP-$PSiO_2$ sensor responses to different interfering molecules, namely, human serum albumin (HSA), cytocrome C (CytC), Lysozyme (Lyz), under the same conditions used for HHb, using a freshly prepared sensor for each experiment.

Repeatability was evaluated by testing the MIP-$PSiO_2$ sensor for HHb detection in triplicate, consecutively performed on the same sensor. Before a new experiment, the MIP was

regenerated through a washing procedure (1 h, stirring) in 50 mM HCl solution prepared in water.

Time stability of the MIP-$PSiO_2$ sensor for HHb detection was evaluated by monitoring the sensor response at HHb 1 $mgmL^{-1}$ at different time intervals, namely, after 1, 7, 15 and 30 days. The sensor was stored in air and subjected before use to a washing procedure (1 h, stirring) in 50 mM HCl solution prepared in water.

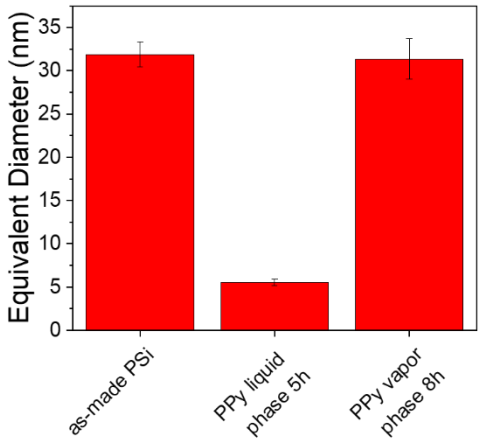

Figure S1. **Pore sizes of $PSiO_2$ scaffolds before and after PPy polymerization.** Equivalent diameter of pores of bare $PSiO_2$ scaffolds and $PSiO_2$ scaffolds after 5 h PPy liquid-phase polymerization and 8 h PPy vapor-phase polymerization. Diameters are extrapolated from top-view SEM images (n=3). Data are presented as mean (± s.d).

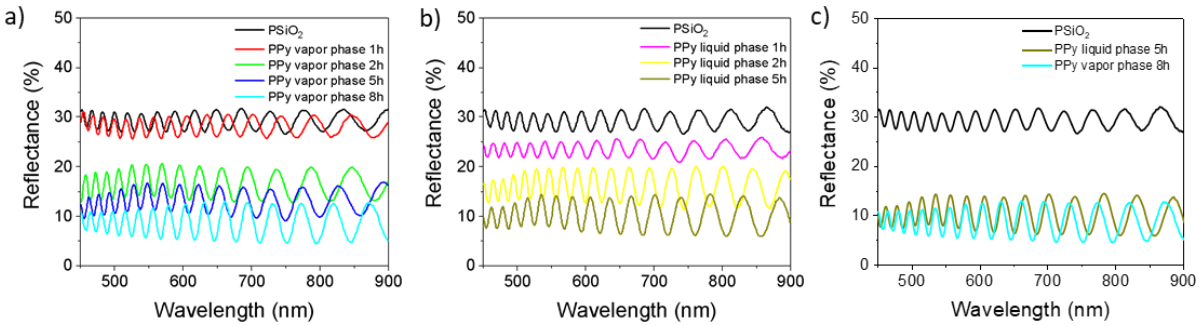

Figure S2. **Optical characterization of $PSiO_2$ scaffolds upon PPy polymerization.** a) Reflectance spectra recorded in air on a $PSiO_2$ scaffold oxidized at 750°C for 1 h before and after PPy vapor-phase deposition for different times. b) Reflectance spectra recorded in air on a $PSiO_2$ scaffold oxidized at 750°C for 1 h before and after PPy liquid-phase deposition for different times. c) Comparison of reflectance spectra recorded in air on $nPSiO_2$ scaffolds oxidized at 750°C for 1h before and after 5h PPy liquid-phase polymerization and 8h PPy vapor-phase polymerization.

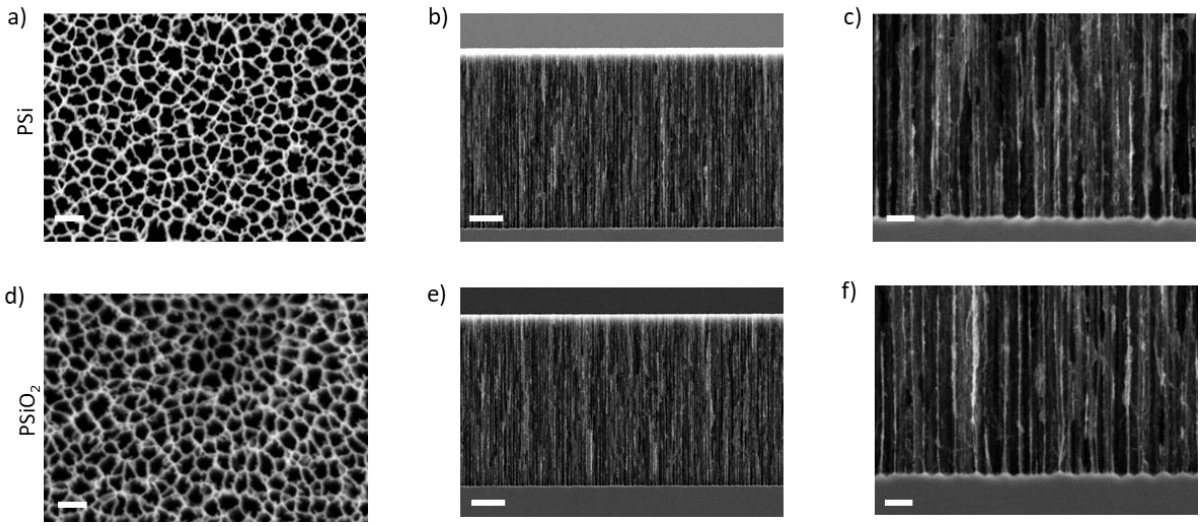

Figure S3. SEM images of PSi scaffolds before and after oxidation to $PSiO_2$. a) Top-view SEM image (magnification 200,000×) of an as-prepared PSi scaffold. Scale bar is 100 nm. b) Cross-section SEM image (magnification 25,000×) of the PSi scaffold in a) Scale-bar is 1 mm. c) Cross-section magnification (100,000×)) of the bottom part of the image in b), which allows to better appreciate the columnar morphology of the pores. Scale-bar is 100 nm. d) Top-view SEM image (magnification 200,000×) of a $PSiO_2$ scaffold, namely PSi scaffold oxidized at 750 °C for 1 h . Scale-bar is 100 nm. e) Cross-section SEM image (magnification 25,000×) of the $PSiO_2$ scaffold in d) Scale-bar is 1 mm. f) Cross-section magnification (100,000×) of the bottom part of the image in e), which allows to better appreciate the columnar morphology of the pores. Scale-bar is 100 nm.

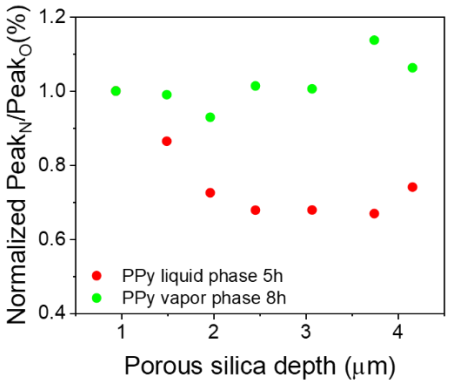

Figure S4. EDX analysis of cross-section of $PSiO_2$ scaffolds after 5 h liquid-phase polymerization and 8 h vapor-phase PPy polymerization. Normalized nitrogen mass percentages measured over pore depth on PPy-coated $PSiO_2$ scaffolds. The peak of oxygen is used as reference for normalization of the signals.

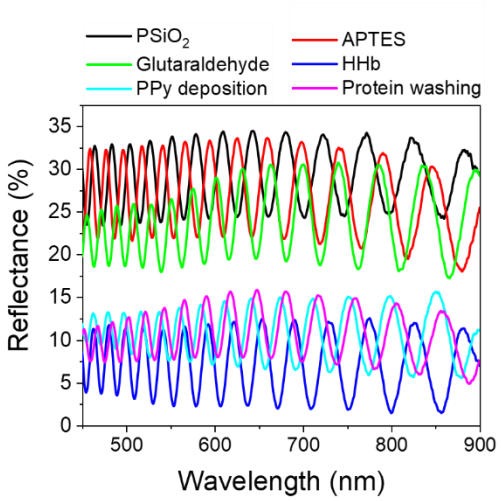

Figure S5. Assessment of the functionalization steps for the synthesis of the MIP for HHb on $PSiO_2$ scaffolds. Reflectance spectra recorded in air on a $nPSiO_2$ scaffold oxidized at 750°C for 1 h before and after all the functionalization steps carried out for the synthesis of a PPy-based MIP for human hemoglobin.

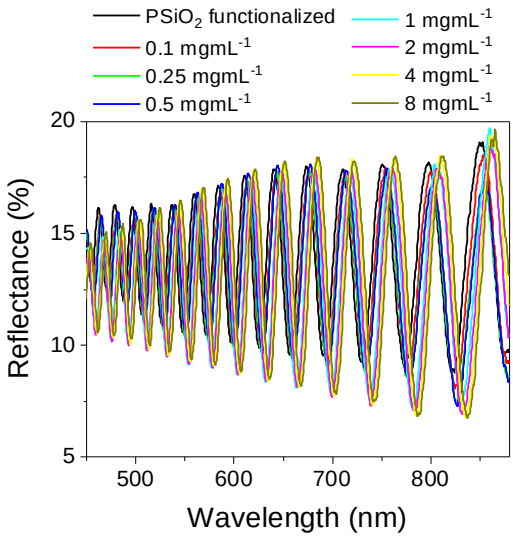

Figure S6. Assessment of the detection of HHb with the MIP-coated $PSiO_2$ scaffolds. Reflectance spectra recorded in air on a MIP-coated $nPSiO_2$ scaffold after exposure to different concentrations of human hemoglobin.

Table S1. XPS data relevant to Si 2p signal on PPy deposited on $PSiO_2$ under different experimental conditions. [a)] Obtained from the comparison of Si 2p area (as an average on

	PPy		PPy-MIP	
	BE (eV)	**Area (%)**	**BE (eV)**	**Area (%)**
C=N	397.9±0.0	3.2±0.3	398.1±0.12	4.2±0.7
N-H	399.8±0.1	71.3±0.5	399.9±0.06	80.3±3.5
$C\text{-}N^+$	401.0±0.3	10.7±0.3	401.3±0.15	10.1±2.7
$C{=}N^+$	402.0±0.1	14.7±0.9	402.5±0.31	5.4±2.3

three points) before and after PPy deposition. [b)] Estimated on Si 2p area after PPy deposition on three points of PSi surface.

Table S2. Binding Energy (BE) and percentage area of components resulting from the fitting of detailed N 1s signal of PPy and MIP-based PPy deposited by 8 h vapor-phase

	Si 2p decrease [%][a)]	**RSD (n=3) [%][b)]**
PPy vapor-phase 1h	15.1	10.7
PPy vapor-phase 8h	35.1	3.5
PPy liquid-phase 5h	97.8	39.9

polymerization on $PSiO_2$ scaffolds. Data are presented as mean (± s.d).

References

(1) Pankratova, N.; Cuartero, M.; Jowett, L. A.; Howe, E. N. W.; Gale, P. A.; Bakker, E.; Crespo, G. A. Fluorinated Tripodal Receptors for Potentiometric Chloride Detection in Biological Fluids. *Biosens. Bioelectron.* **2018**, *99* (July 2017), 70–76. https://doi.org/10.1016/j.bios.2017.07.001.

(2) Sailor, M. J. *Porous Silicon in Practice: Preparation, Characterization and Applications*; Wiley-VCH, 2012. https://doi.org/10.1002/9783527641901.

(3) Ruminski, A. M.; Barillaro, G.; Chaffin, C.; Sailor, M. J. Internally Referenced Remote Sensors for HF and Cl2 Using Reactive Porous Silicon Photonic Crystals. *Adv. Funct. Mater.* **2011**, *21* (8), 1511–1525. https://doi.org/10.1002/ADFM.201002037.

(4) Kharat, H. J.; Kakde, K. P.; Savale, P. A.; Datta, K.; Ghosh, P.; Shirsat, M. D. Synthesis of Polypyrrole Films for the Development of Ammonia Sensor. *Polym. Adv. Technol.* **2007**, *18* (5), 397–402. https://doi.org/10.1002/PAT.903.

(5) Perruchot, C.; Chehimi, M. M.; Delamar, M.; Cabet-Deliry, E.; Miksa, B.; Slomkowski, S.; Khan, M. A.; Armes, S. P. Chemical Deposition and Characterization of Thin Polypyrrole Films on Glass Plates: Role of Organosilane Treatment. *Colloid Polym. Sci. 2000 27812* **2000**, *278* (12), 1139–1154. https://doi.org/10.1007/S003960000372.

(6) Kim, J.; Sohn, D.; Sung, Y.; Kim, E. R. Fabrication and Characterization of Conductive Polypyrrole Thin Film Prepared by in Situ Vapor-Phase Polymerization. *Synth. Met.* **2003**, *132* (3), 309–313. https://doi.org/10.1016/S0379-6779(02)00462-9.

(7) Niu, H.; Zhou, H.; Wang, H.; Lin, T.; Niu, H.; Zhou, H.; Wang, H.; Lin, T. Polypyrrole-Coated PDMS Fibrous Membrane: Flexible Strain Sensor with Distinctive Resistance Responses at Different Strain Ranges. *Macromol. Mater. Eng.* **2016**, *301* (6), 707–713. https://doi.org/10.1002/MAME.201500447.

(8) Zhu, M.; Lerum, M. Z.; Chen, W. How to Prepare Reproducible, Homogeneous, and Hydrolytically Stable Aminosilane-Derived Layers on Silica. *Langmuir* **2012**, *28* (1), 416–423. https://doi.org/https://doi.org/10.1021/la203638g.

(9) Acres, R. G.; Ellis, A. V.; Alvino, J.; Lenahan, C. E.; Khodakov, D. A.; Metha, G. F.; Andersson, G. G. Molecular Structure of 3-Aminopropyltriethoxysilane Layers Formed on Silanol-Terminated Silicon Surfaces. *J. Phys. Chem. C* **2012**, *116* (10), 6289–6297. https://doi.org/https://doi.org/10.1021/jp212056s.

(10) Pasternack, R. M.; Amy, S. R.; Chabal, Y. J. Attachment of 3-(Aminopropyl)Triethoxysilane on Silicon Oxide Surfaces: Dependence on Solution Temperature. *Langmuir* **2008**, *24* (22), 12963–12971. https://doi.org/https://doi.org/10.1021/la8024827.

(11) Yuan, H.; Mullett, W. M.; Pawliszyn, J. Biological Sample Analysis with Immunoaffinity Solid-Phase Microextraction. *Analyst* **2001**, *126* (8), 1456–1461. https://doi.org/https://doi.org/10.1039/b101854j.

(12) Jannat, M.; Yang, K. L. Immobilization of Enzymes on Flexible Tubing Surfaces for Continuous Bioassays. *Langmuir* **2018**, *34* (47), 14226–14233. https://doi.org/https://doi.org/10.1021/acs.langmuir.8b02991.

(13) Umpleby, R. J.; Baxter, S. C.; Chen, Y.; Shah, R. N.; Shimizu, K. D. Characterization of Molecularly Imprinted Polymers with the Langmuir - Freundlich Isotherm. *Anal. Chem.* **2001**, *73* (19), 4584–4591. https://doi.org/https://doi.org/10.1021/ac0105686.

(14) Ansell, R. J. Characterization of the Binding Properties of Molecularly Imprinted Polymers. In *Advances in Biochemical Engineering/Biotechnology*; Springer Science and Business Media Deutschland GmbH, 2015; Vol. 150, pp 51–93. https://doi.org/10.1007/10_2015_316.